Available online at www.sciencedirect.com

ScienceDirect

Ceramics International 41 (2015) 5380–5386

CERAMICS INTERNATIONAL

www.elsevier.com/locate/ceramint

Influences of secondary phases on ferroelectric properties of $Bi(Na,K)TiO_3$ ceramics

L. Ramajo[a,*], J. Camargo[a], F. Rubio-Marcos[b], M. Castro[a]

[a]*Institute of Research in Materials Science and Technology (INTEMA), Juan B. Justo 4302, Mar del Plata B7608FDQ, Argentina*
[b]*Electroceramic Department, Instituto de Cerámica y Vidrio, CSIC, Kelsen 5, 28049 Madrid, Spain*

Received 11 September 2014; received in revised form 17 November 2014; accepted 17 December 2014
Available online 24 December 2014

Abstract

The effect of secondary phases on ferroelectric properties of $Bi_{0.5}(Na_{0.8}K_{0.2})_{0.5}TiO_3$ (BNKT) is studied. Ceramic powders are prepared by the solid-state reaction method where the influence of different sintering temperatures is also studied. Then, samples are characterized by X-ray diffraction (XRD), Raman microspectroscopy, Scanning Electron Microscopy and impedance spectroscopy. Through XRD and Raman results, the perovskite structure is detected; together with small peaks corresponding to a secondary phase associated with a $K_{2-x}Na_xTi_6O_{13}$-based phase. The secondary phases amount increases with the sintering temperature, yielding different combinations of $K_{2-x}Na_xTi_6O_{13}$- and $Bi_{0.5}(Na_{1-y}K_y)_{0.5}TiO_3$-based phases. Moreover, the content of the secondary phase improves the d_{33} piezoelectric constant and dielectric properties of BNKT ceramics. These results can benefit the understanding of BNKT ceramics and the expanding of their applications range.

Keywords: A. Powders: solid state reaction; C. Ferroelectric properties; C. Piezoelectric properties; D. Perovskites

1. Introduction

Piezoelectric ceramics are attractive and important materials that are used for many applications such as sensors, actuators, and transducers due to their electromechanical properties. In this way, lead titanate–zirconate piezoceramics are the most widely used materials for these devices although the toxicity of lead is a serious threat to human health and environment [1]. Thus, considerable effort, regulations and restrictions on using hazardous substances in electronics devices have been devoted towards the development of lead-free piezoelectric ceramics.

Recent reports on lead-free piezo-ceramics can be categorized into two main perovskite families: $(K,Na)NbO_3$ (KNN) and $(Na,Bi)TiO_3$ (NBT) or $(K,Bi)TiO_3$ (KBT) [2–4]. The KNN phase was discovered in the late 1950s, with a piezoelectric coefficient (d_{33}) of about 80 pC/N and a Curie temperature of 420 °C close to the morphotropic phase boundary (MPB) [5]. Nevertheless, it is difficult to obtain pure KNN-based ceramics with a high density and great piezoelectric performance.

Sodium bismuth titanate $Na_{0.5}Bi_{0.5}TiO_3$ (BNT) with a relatively large remnant polarization at room temperature and a relatively high Curie temperature could be considered as another promising candidate to lead-free piezoelectric ceramics [6]. In a $Bi_{0.5}Na_{0.5}TiO_3$–$Bi_{0.5}K_{0.5}TiO_3$ (BNKT) system, when Na^+ is partially substituted by K^+ on the A-site of BNT, the system shows high strain and ferroelectric properties [7]. The high strains observed in the BNKT system under a strong electric field are due to a 90° domain reorientation [8] increasing its coercive field. Consequently, this fact hinders the development of desired piezoelectric properties. Therefore, a number of studies have been carried out to improve electrical properties of BNT by the formation of solid solutions with other ABO_3 perovskites [9–11].

Herein, we present a simple method to prepare $Bi_{0.5}(Na_{1-x}K_x)_{0.5}TiO_3$-based lead-free piezoelectric ceramics by the solid-state reaction method using a previous mechanochemical activation step of reagents. By this procedure two chief achievements were made: one is the clarification on the effect of the sintering temperature on the structure, microstructure, dielectric

*Corresponding author.
E-mail address: lramajo@fi.mdp.edu.ar (L. Ramajo).

http://dx.doi.org/10.1016/j.ceramint.2014.12.100
0272-8842/

and piezoelectric properties of $Bi_{0.5}(Na_{0.8}K_{0.2})_{0.5}TiO_3$-based system, while the other is the discussion on the formation of a secondary phase during the sintering route. It should be emphasized that when the sintering temperature is increased, the secondary phase content increases. As a result, this phase improves the piezoelectric and dielectric properties of these ceramics.

2. Material and methods

$Bi_{0.5}(K_{0.2}Na_{0.8})_{0.5}TiO_3$ was synthesized through solid state reaction, using K_2CO_3 and Na_2CO_3 (Cicarelli 99.99%; Argentina), Bi_2O_3 (Aldrich 99.8%; USA) and TiO_2 (Aldrich 99.9%; USA). Powders were mixed and milled using zirconia balls in an alcoholic medium in a planetary mill (Fritsch, Pulverisette 7, 1450 rpm) for 5 h. Powders were dried and calcined at 700 °C for 2 h. The resulting powders were milled again, pressed into disks and sintered at 1075–1150 °C for 2 h (hereafter, denoted as BNKT-1075, 1100, 1125 and 1150).

Crystalline phases were characterized by X-ray diffraction (XRD) (Philips PW1830), using CuKα radiation. Density values were determined using the Archimedes method. Microstructures were evaluated on polished and thermally etched samples using a Field Emission Scanning Electron Microscope, FE-SEM (Hitachi S-4700) equipped with energy dispersive spectroscopy, EDS. The average grain size was determined from FE-SEM micrographs by an image-processing and analyzing program (Leica Qwin, Leica Microsystems Ltd., Cambridge, England) considering more than 100 grains in each measurement.

To characterize the dielectric and piezoelectric properties, the ceramic specimens were polished and coated with silver paint on the upper and bottom surfaces and fired at 700 °C for 20 min. The temperature dependence of permittivity was measured using an impedance analyzer (HP4294A, Agilent) in the frequency range 100 Hz–1 MHz and the temperature range 30–500 °C, using a heating rate of 2 °C min^{-1}. In order to test the piezoelectric constant, the samples were polarized under a direct current (dc) electric field of 40 kV/cm in a silicon oil bath at 25–100 °C for 30 min. The piezoelectric coefficient d_{33} was measured using a piezo d_{33} meter (YE2730A d_{33} METER, APC International, Ltd., USA). Finally, the ferroelectric nature of these ceramics was determined using a hysteresis meter (RT 6000 HVS, RADIANT Technologies).

Raman analyses were performed employing a Confocal Raman Microscope (Witec alpha-300R). Ceramic samples were polished and thermally etched at 950 °C for 5 min. Raman spectra were obtained using 532 nm excitation laser and a 100× objective lens (NA=0.95). The incident laser power was 40 mW. The optical diffraction resolution of the Confocal Microscope was limited to about ~200 nm laterally and ~500 nm vertically. The Raman spectral resolution of the system was 0.02 cm^{-1}. The sample was mounted on a piece-driven scan platform having 4 nm lateral and 0.5 nm vertical positional accuracy. The microscope base was also equipped with an active vibration isolation system, active 0.7–1000 Hz. Collected spectra were analyzed using the Witec Control Plus Software.

3. Results and discussion

As mentioned in the experimental section, the ceramics were sintered at temperatures between 1075 and 1150 °C in order to assess the structure of the BNKT system. The X-ray diffraction patterns of ceramics sintered at temperatures from 1075 °C to 1150 °C are shown in Fig. 1. The diffraction patterns correspond to a perovskite-phase. At higher sintering temperature, the pattern also reveals a minor secondary-phase, which was assigned to $K_{2-x}Na_xTi_6O_{13}$ (JCPDS Nos. 40-0403 and 74-0275) with monoclinic structure (hereafter, denoted as KNT). The apparition of this secondary phase is the result of slight changes in the stoichiometric ratio due to highly volatile alkaline elements during the sintering process [12]. It is worth pointing out that it has been possible to locate the coexistence between a rhombohedral symmetry, R, and a tetragonal symmetry, T, (as shown in insets of Fig. 1) as revealed by the X-ray diffraction patterns. According to these results, the splitting of the peaks centered at ~40° and 46° (2θ) is simultaneously observed [13], corresponding to (111)/(111) lattice planes of the rhombohedral symmetry and (002)/(200) lattice planes of the tetragonal symmetry, respectively (see insets of Fig. 1).

In order to obtain additional information about the structural evolution by Raman images (Fig. 2a–d), the average Raman spectra (Fig. 2e) and the secondary phase Raman spectra (Fig. 2f) were recorded for sintered samples. In the average Raman spectra, six vibration bands corresponding to BNKT are observed in all sintered samples. The amplitude and overlapping of the Raman bands reflect the strong anharmonicity and disorder inherent to A-sites. Moreover, new peaks related to a secondary phase assigned to KNT phase can be observed in Fig. 2e. Therefore, Fig. 2e presents the average Raman spectrum corresponding to secondary phase.

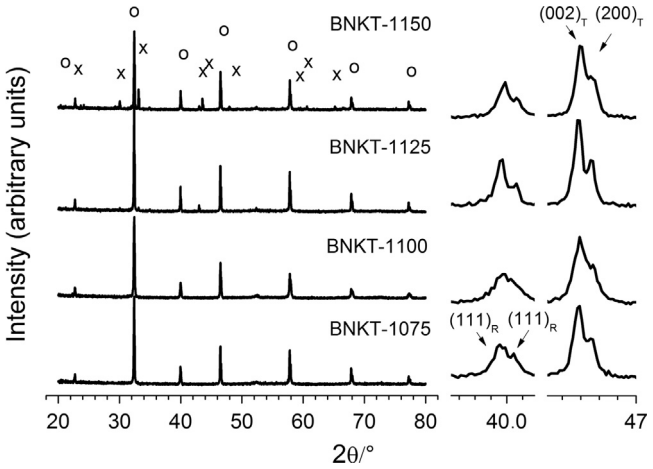

Fig. 1. XRD patterns of sintered samples: (o) peaks corresponding to BNKT phase and (x) peaks associated with a secondary phase (KNT). The insets of the figure show the magnified XRD diffraction pattern in the 2θ range 39–41° and 46–47° of each system. (R: rhombohedral symmetry and T: tetragonal symmetry).

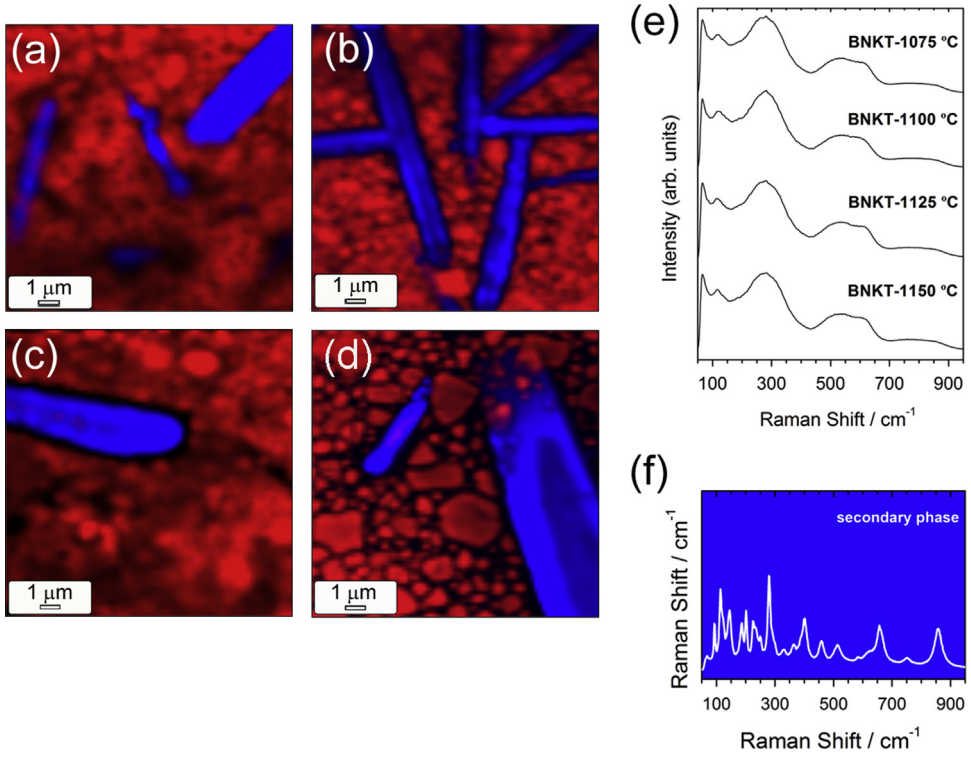

Fig. 2. Detection of the secondary phase observed in the BNKT ceramics sintered at different temperatures through Confocal Raman Spectroscopy: (a) 1075 °C; (b) 1100 °C; (c) 1125 °C and (d) 1150 °C. The Raman image of BNKT samples exhibiting the location of secondary phase is shown in blue areas. The Raman image is derived by summing the total spectral pixel intensity from 50 cm^{-1} to 950 cm^{-1}. The secondary phases signaled in blue, whereas the BNKT perovskite phases are marked in red. (e, f) Average Raman spectra of BNKT and secondary phase, respectively. (For interpretation of the references to color in this figure legend, the reader is referred to the web version of this article.)

The identification and quantification of secondary phases can be approached by Confocal Raman Microscopy (CRM). It is worth pointing out that it has been possible to locate the secondary phase (marked in blue regions in Fig. 2a–c) as revealed by the CRM imaging. In this way, Fig. 2f shows the Raman spectra of this secondary phase, which could be attributed to the different reagent reactivity.

In the average Raman spectra, peaks below 500 cm^{-1} could be attributed to the K–O–Ti stretching vibration. Peaks at about 655 cm^{-1} have been assigned to the Ti–O–Ti stretch in edge-shared TiO_6. Peaks near 870 cm^{-1} are reported for a short Ti–O stretching vibration in distorted TiO_6. Weak peaks at around 240 and 400 cm^{-1} characteristic of the K–O–Ti containing short Ti–O bonds are also observed. Although secondary phases are not detected through XRD patterns at the lowest sintering temperature, Raman spectra confirm the formation of a secondary phase with a composition close to $K_{2-x}Na_xTi_6O_{13}$ in all samples [14]. This could imply that the secondary phase is well below the XRD sensitivity by low amount or low crystallinity.

The FE-SEM images, shown in Fig. 3a–d, illustrate the microstructure of the BNKT ceramics, which were sintered at different temperatures ranging from 1075 to 1150 °C for 2 h.. From Fig. 3a.1 and d.1 it can be observed that the ceramics have a dense microstructure. The FE-SEM micrographs show the typical BNKT morphology consisting of very small faceted grains, see Fig. 3a.2–d.2, although the sintering temperature affects the grain size and the content of the secondary phase. Grain size distributions, GSDs, of the ceramic samples are shown in the insets of Fig. 3a.1–d.1. In the GSDs, it can also be observed that the grain size increases with the sintering temperature. The average grain size (AGS) increases from $\sim 0.40 \pm 0.15$ μm in the ceramic at a lower sintering temperature (1075 °C), to $\sim 0.92 \pm 0.40$ μm for the ceramic sintered at 1150 °C. The evolution of the AGS as a function of the sintering temperature is displayed in Fig. 3f. With increasing temperature, the AGS reveals a linear increase.

Furthermore, in the same manner as the AGS evolves, the secondary phase content increases with thermal treatment. Fig. 3a.3–d.3 shows a detail of the morphology of the secondary phase, which is present in the form of rods. This phase has a composition close to $K_{2-x}Na_xTi_6O_{13}$ as detected by XRD and Raman microspectroscopy.

Fig. 4a and b shows the temperature-dependent behavior of dielectric permittivity and dielectric loss of BNKT-1075 to 1150. The curves exhibit two distinct anomalies for all samples, which correspond to the depolarization temperature (T_d) and maximum dielectric constant temperature (T_m) around 120 ° C and 300 °C, respectively. The curves for different samples look similar, all displaying two-phase transition at T_d and T_m. The maximum dielectric permittivity increased with the sintering temperature, due to the grain size raise and density improvement. Moreover, the dielectric anomaly peaks at T_m for all the ceramics are relatively broad, indicating that the phase transition at T_m is a diffuse phase transition.

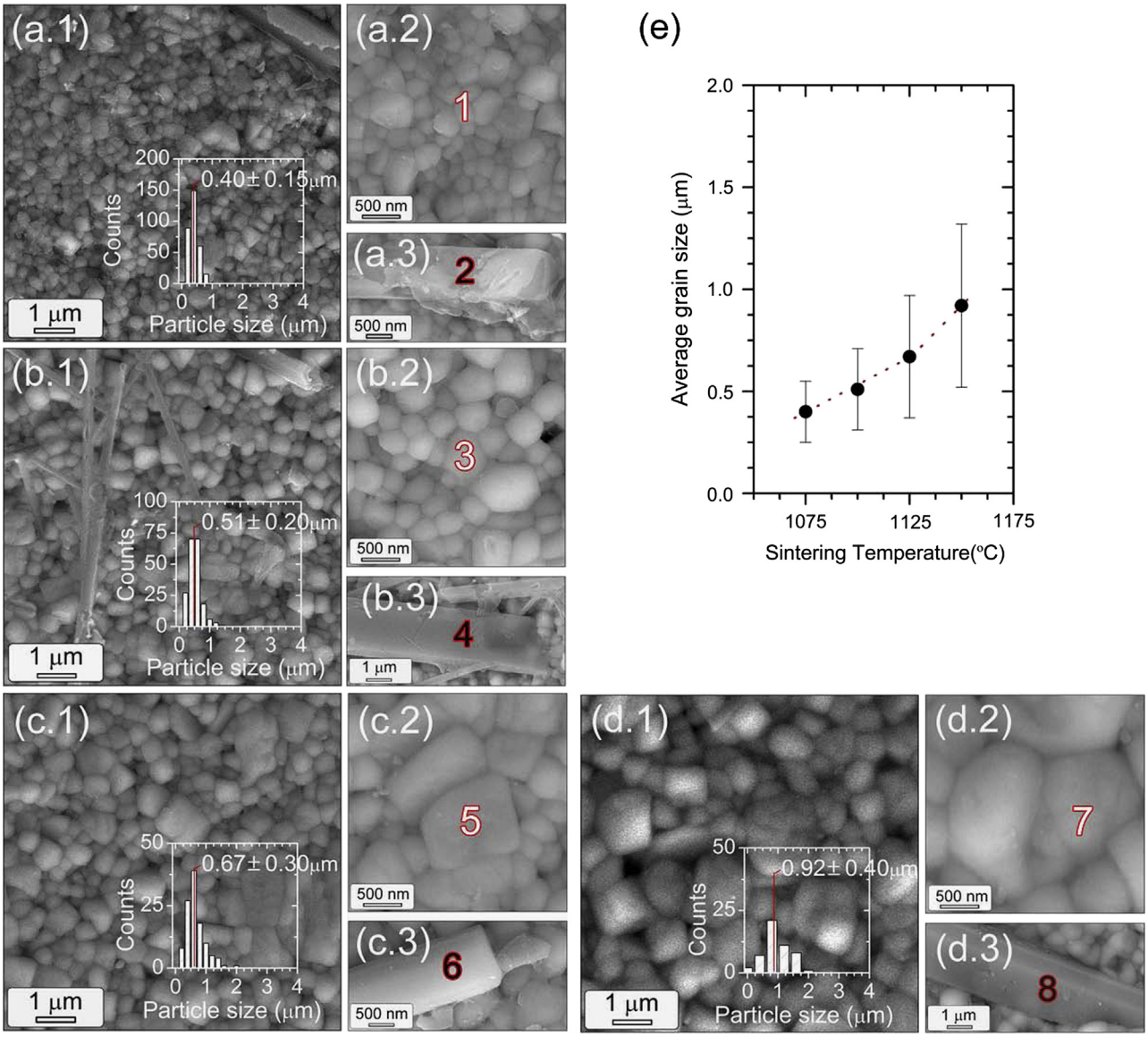

Fig. 3. FE-SEM images of BNKT (a) 1075, (b) 1100, (c) 1125, and (d) 1150. The insets of Fig. 1(a, d) show the grain-size distributions of BNKT ceramics. Figs. 2 (a–d and a.3–d.3) show details of the morphology of BNKT grains and of the secondary phase. (e) Evolution of the average grain size as a function of the sintering temperature.

In Fig. 4(c) it is shown that at low frequencies, permittivity increases drastically, when frequency decreases, as a consequence of polarization between grains characteristic of the polycrystalline materials. Additionally, from Fig. 4c and d a relaxation process at high frequency (~8 MHz), which is associated with a dipolar relaxation phenomena can be observed. In these samples, the improvement in the real permittivity value with the sintering temperature could be related to the secondary phase formation, the grain size increase and the densification degree.

In order to observe the temperature and frequency dependence, Fig. 5 shows the relative permittivity as a function of temperature of sample BNKT-1100, at various frequencies. The shift in the maximum temperature depending on frequency and the diffusive phase transition for all samples suggest the relaxor-like behavior of these ceramics. The broadening of the real premittivity peak around the dielectric maximum temperature may be due to compositional fluctuations occurring at A- and B-sites of the perovskite unit cell, as a result of the secondary phase formation.

It is known that K/Na ratio control is critically important for achieving high piezoelectricity in the BNKT system, but the quantitative measurement of K and Na elements is complex. However, we have used EDS analysis for semi-quantitative determination of K/Na ratios in resultant BNKT ceramics. EDS analysis was carried out on the ceramics (Fig. 3) to identify the grain and the secondary phase compositions.

The matrix grains (points marked as 1, 3, 5 and 7 in Fig. 3a.2, b.2, c.2, and d.2, respectively) have a nominal composition ratio Na/K ~5.7, 5.7, 5.8 and 6.4, for the samples sintered at 1075, 1100, 1125 and 1150 °C, respectively. These values are higher than the nominal ratio of 4.0, and this difference was higher in the matrix grains or when the

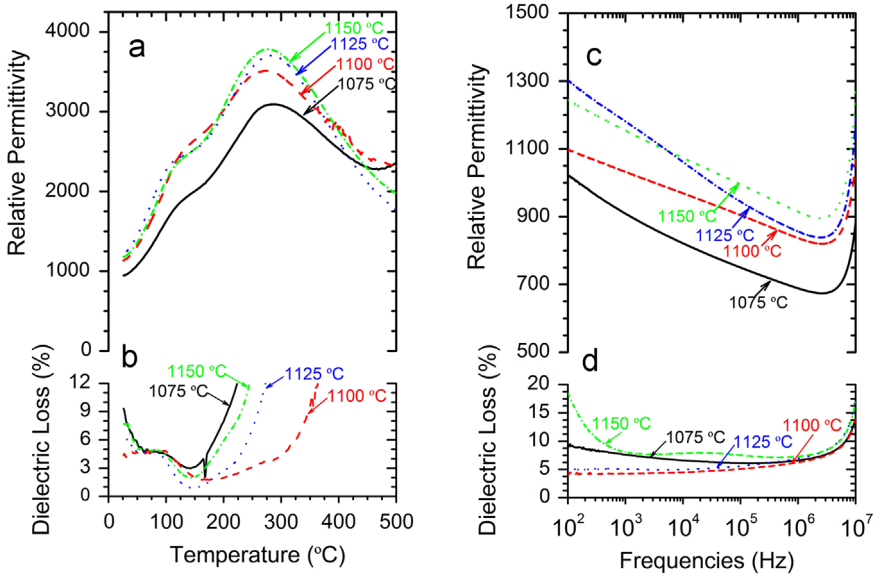

Fig. 4. (a, b) Temperature-dependence at 100 kHz, and (c, d) frequency-dependent at room temperature of dielectric permittivity (a, c) and dielectric loss (b, d) of BNKT-1075 to 1100.

sintering temperature exceeds 1100 °C (see more information about the EDS spectra in Supporting material). The energy dispersion spectrum analysis (EDS) also reveals that the atomic percentages of elements change within the different grains. In this way, the composition analyses of all systems are summarized in Table 1.

In the secondary phase, the detected composition by the EDS shows lower concentration of Na, Bi, and Ti cations, while the atomic percentage of K presents higher values than those detected in the BKNT matrix grains. According to EDS analysis, the secondary phase composition (point signaled as 2, 4, 6 and 8 in Fig. 3a.3, b.3, c.3, and d.3, respectively) is quite similar to $K_{2-x}Na_xTi_6O_{13}$ (KNT), although our results reveal that the KNT phase grains present slight variations in Na-composition. Considering, then, the aforementioned observations in the structural characterization section (XRD and CRM), the constitution of the secondary phase modifies the composition of the main phase.

In addition, a maximum in dielectric loss between 100 and 150 °C is observed in Fig. 5, and corresponds to the depolarization temperature (T_d). There was still a controversy in the interpretation of T_d but it was long believed to be the ferroelectric to antiferroelectric phase transition point on heating [15]. However, T_d was recently interpreted as the nonergodic relaxor (NR) to ergodic relaxor (ER) phase transition point [10]. From this explanation, the occurring of depolarization in BNT-based ceramics is due to the phase transition from long-range ferroelectric order to the relaxor state upon heating, not a structure phase transition from a low symmetry to a higher symmetry.

In addition, Table 1 shows the density values of these samples. According to the density values, samples sintered at 1100 °C present the maximum value of the complete set of samples, although the highest the piezoelectric coefficient (d_{33}) is observed in samples with high secondary phases content (BNKT-1150). The formation of this phase could be

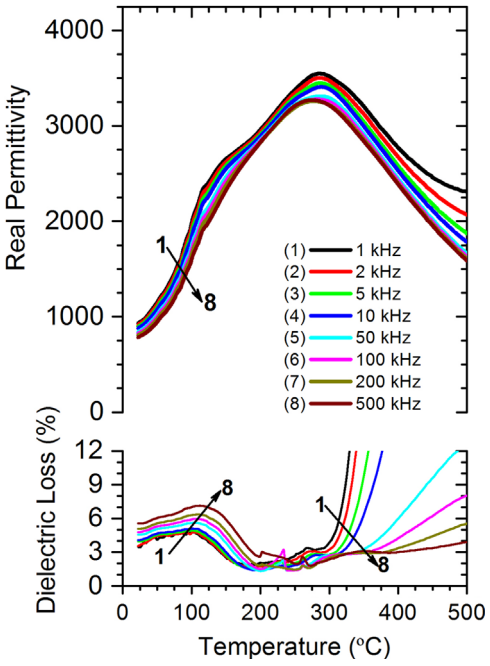

Fig. 5. Relative permittivity (top) and dielectric loss (bottom) vs. temperature curves of BNKT-1100 obtained at different frequencies.

related to the mechanochemical activation of powders in the solid-state reaction method. The d_{33} values registered in all samples are lower than values obtained in BNKT [16], which suggest that polarization conditions were not enough to obtain the best properties or that the BNKT presents high cubic phase content.

Finally, hysteresis loops of BNKT-1075 to 1150 are shown in Fig. 6a–d. At room temperature, the BNKT-1075 sample shows a remnant polarization (P_r) 8.0 μC/cm^2, which increases to 9.8, 20.1 and 19.8 μC/cm^2 with sintering temperature rise, while the

Table 1
The table shows the composition in the regions shown in Fig. 3 derived from EDS spectra (see Supporting material), which represents the atomic percentages of elements. Moreover, the table presents the relative density (ρ) and piezoelectric coefficient (d_{33}) of the BNKT ceramic samples. Theoretical density 5.84 g/cm^3 [19], dielectric constant 130 pC/N [19].

Sample		O	Na	K	Bi	Na/K	Ti	ρ (g/cm^3)	d_{33} (pC/N)
BNKT-1075	**1**	45.49	10.90	1.91	15.73	5.70	25.97	5.64	30
	2	43.72	3.07	10.26	1.11	0.30	41.84		
BNKT-1100	**3**	43.82	10.72	1.87	16.23	5.73	27.35	5.79	50
	4	46.79	2.43	9.85	0.44	0.25	40.49		
BNKT-1125	**5**	46.48	10.52	1.81	15.10	5.81	26.12	5.65	90
	6	58.89	3.51	6.88	0.81	0.51	29.91		
BNKT-1150	**7**	45.47	11.72	1.83	15.24	6.41	25.75	5.59	100
	8	49.16	3.02	9.18	0.57	0.33	38.07		

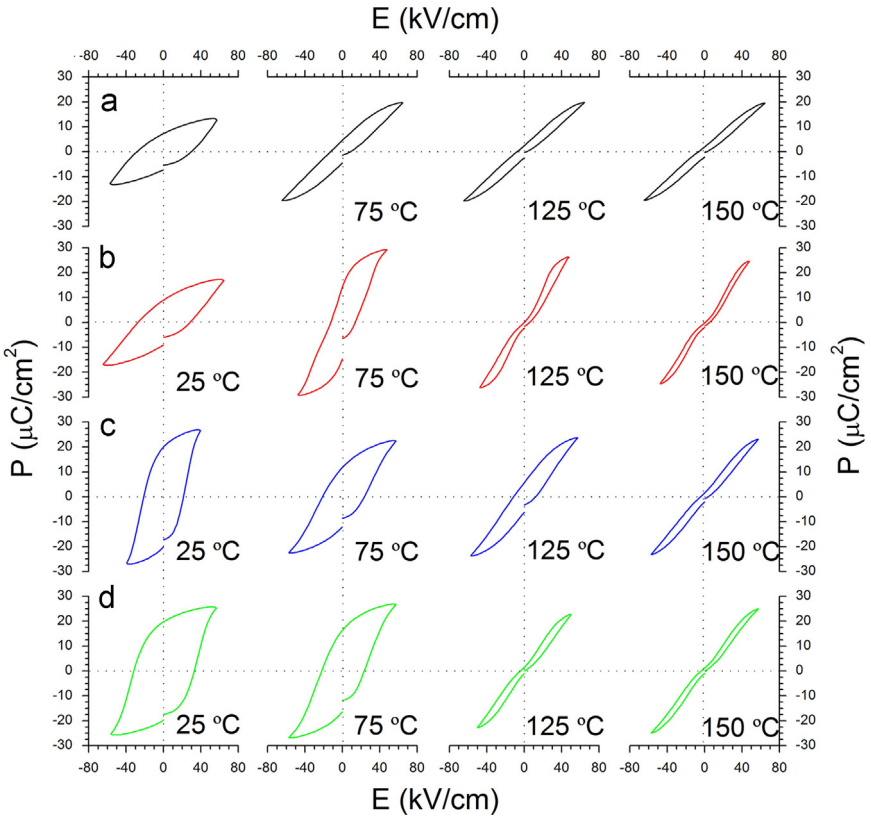

Fig. 6. Saturated polarization hysteresis of BNKT- (a) 1075, (b) 1100, (c) 1125, and (d) 1150 ceramics as a function of temperature, measured at 100 Hz.

coercive electric field (E_c), and the saturation polarization values (P_s) are 29.1, 28.8, 21.5 and 31.6 kV/cm and 13.2, 17.0, 26.9 and 25.8 μC/cm^2, for BNKT-1075, 1100, 1125 and 1150, respectively. Further increase in temperature makes the loops slim, and close to 125 °C an anomaly is perceptible, which corresponds to the depolarization temperature T_d. Thus, the polarization hysteresis behavior as a function of temperature exhibited a narrowing of the hysteresis loops with the temperature, resulting in a significant decrease in the coercive field. Above 125 °C, in addition to the decrease in coercive field, the loops became pinched, resulting in a massive reduction in remanent polarization. The observation of pinched-type loop at high temperature may be due to the weakening of nonergodic relaxor (NR) state and enhancing ergodic relaxor (ER) state. The constricted or pinched-type *P–E* loop have previously been observed in BNT-based ceramics at high temperature [10,17]. The temperature at which this pinching initiates corresponds to the onset of the frequency dispersion in the dielectric response at around 100 °C [18]. These results also confirm the depolarization temperature observed in the permittivity analysis, as shown in Fig. 4a.

Taking into account the increase in the coercive electric field values, a hardness effect on the ferroelectric properties of BNKT with the increase of the KNT secondary phase amount is detected. This result could be associated with the densification degree, and the anchoring effect of grain boundaries which limit the polarization of materials, and increase the coercive field of the samples and the energy involved in changing the polarization of the material.

4. Conclusions

The effect of different secondary phase contents in particular $K_{2-x}Na_xTi_6O_{13}$, on ferroelectric properties of $Bi_{0.5}(Na_{0.8}K_{0.2})_{0.5}TiO_3$ (BNKT) ceramics obtained by the conventional mixed oxide method has been reported. Ceramic powders are prepared using different sintering temperatures in order to obtain different combinations of $K_{2-x}Na_xTi_6O_{13}$ and $Bi_{0.5}(Na_{1-y}K_y)_{0.5}TiO_3$. The structural and microstructural analyses show the formation of main perovskite-type structure and a secondary phase with a composition close to $K_{2-x}Na_xTi_6O_{13}$. Thus, when the sintering temperature is increased, the secondary phase content increases and, interestingly, this phase improves the piezoelectric and dielectric properties of these ceramics. The Confocal Raman methodology allows obtaining images of the KNT secondary phase with high spatial resolution, which is not detected through XRD patterns at the lowest sintering temperature. Therefore, by means of the Raman mapping it is possible to obtain a complete and detailed study of the KNT secondary phase, and evaluate the interaction between the BNKT system and the KNT phase, which is not simple by other techniques. The *P–E* loops demonstrate that the BNKT ceramics gradually change from the ferroelectric behavior in a non-polar phase passing through an intermediate stage, which presents both ferroelectric and non-polar characteristics. The maximum dielectric constant temperature gradually decreases with increasing $K_{2-x}Na_xTi_6O_{13}$ content, while the dielectric constant increase. As a result, we believe that knowing the secondary phases origin can be a further advantage in the developing BNKT based materials.

Acknowledgments

The authors are grateful to L′Oréal-CONICET, ANPCyT, University of Mar del Plata (Argentina) and to MINECO (Spain) Project MAT2013-48009-C4-1-P for the financial support provided for this research. Dr. F. Rubio-Marcos is also indebted to MINECO (Spain) for a "Juan de la Cierva" contract (ref: JCI-2012-14521), which is cofinanced with FEDER funds.

Appendix A. Supporting information

Supplementary data associated with this article can be found in the online version at http://dx.doi.org/10.1016/j.ceramint.2014.12.100.

References

[1] J. Rodel, W. Jo, K.T.P. Seifert, E.M. Anton, T. Granzow, D. Damjanovic, Perspective on the development of lead-free piezoceramics, J. Am. Ceram. Soc. 92 (2009) 1153–1177.

[2] X.P. Jiang, L.Z. Li, M. Zeng, H.L.W. Chan, Dielectric properties of Mn doped $(Na_{0.8}K_{0.2})_{0.5}Bi_{0.5}TiO_3$ ceramics, Mater. Lett. 60 (2006) 1786–1790.

[3] J.B. Lim, S.J. Zhang, J.H. Jeon, T.R. Shrout, (K,Na)NbO_3-based ceramics for piezoelectric hard lead-free materials, J. Am. Ceram. Soc. 93 (2010) 1218–1220.

[4] T. Takenaka, K. Maruyama, K. Sakata, (Bi,Na)TiO_3–$BaTiO_3$ system for lead free piezoelectric ceramics, Jpn. J. Appl. Phys. 30 (1991) 2236–2239.

[5] J.B. Lim, D. Suvorov, J.H. Jeon, Ferroelectric Bi(Na,K)TiO_3-based materials for lead-free piezoelectrics, Ceram. Int. 38S (2012) S355–S358.

[6] D. Lin, K.W. Kwok, H.L.W. Chan, Structure and electrical properties of $Bi_{0.5}Na_{0.5}TiO_3$–$BaTiO_3$–$Bi_{0.5}Li_{0.5}TiO_3$ lead-free piezoelectric ceramics, Solid State Ion. 178 (2008) 1930–1937.

[7] A. Ullah, R.A. Malik, A. Ullah, D.S. Lee, S.J. Jeong, J.S. Lee, I.W. Kim, C.W. Ahn, Electric-field-induced phase transition and large strain in lead-free Nb-doped BNKT–BST ceramics, J. Eur. Ceram. Soc. 34 (2014) 29–35.

[8] K.N. Pham, A. Hussain, C.W. Ahn, I.W. Kim, S.J. Jeong, J.S. Lee, Giant strain in Nb-doped $Bi_{0.5}(Na_{0.82}K_{0.18})_{0.5}TiO_3$ lead-free electromechanical ceramics, Mater. Lett. 64 (2010) 2219–2222.

[9] M. Jiang, X. Liu, C. Liu, Effect of $BiFeO_3$ additions on the dielectric and piezoelectric properties of $(K_{0.44}Na_{0.52}Li_{0.04})(Nb_{0.84}Ta_{0.1}Sb_{0.06})O_3$ ceramics, Mater. Res. Bull. 45 (2010) 220–223.

[10] B. Wang, L. Luo, F. Ni, P. Du, W. Li, H. Chen, Piezoelectric and ferroelectric properties of $(Bi_{1-x}Na_{0.8}K_{0.2}La_x)_{0.5}TiO_3$ lead-free ceramics, J. Alloys Compd. 526 (2012) 79–84.

[11] C.R. Zhou, L.Y. Chai, Dielectric and piezoelectric properties of $Bi_{0.5}(Na_{0.82}K_{0.18})_{0.5}TiO_3$–$LiSbO_3$ lead-free piezoelectric ceramics, Bull. Mater. Sci. 34 (2011) 933–936.

[12] L. Ramajo, M. Castro, F. Rubio-Marcos, J. Fernandez-Lozano, Influence of MoO_3 on electrical and microstructural properties of $(K_{0.44}Na_{0.52}Li_{0.04})(Nb_{0.86}Ta_{0.10}Sb_{0.04})O_3$, J. Mater. Sci.: Mater. Electron. 24 (2013) 3587–3593.

[13] H.-B. Lee, D.-J. Heo, R.A. Malik, C.-H. Yoon, H.-S. Han, J.-S. Leen, Lead-free $Bi_{1/2}(Na_{0.82}K_{0.18})_{1/2}TiO_3$ ceramics exhibiting large strain with small hysteresis, Ceram. Int. 39 (2013) S705–S708.

[14] X. Meng, D. Wang, J. Liu, B. Lin, Z. Fu, Effects of titania different phases on the microstructure and properties of $K_2Ti_6O_{13}$ nanowires, Solid State Commun. 137 (2006) 146–149.

[15] X.P. Jiang, L.Z. Li, M. Zeng, H.L.W. Chan, Dielectric properties of Mn-doped $(Na_{0.8}K_{0.2})_{0.5}Bi_{0.5}TiO_3$ ceramics, Mater. Lett. 60 (2006) 1786–1790.

[16] Y.R. Zhang, J.F. Li, B.P. Zhang, Enhancing electrical properties in NBT–KBT lead-free piezoelectric ceramics by optimizing sintering temperature, J. Am. Ceram. Soc. 91 (2008) 2716–2719.

[17] J.-F. Trelcat, C. Courtois, M. Rguiti, A. Leriche, P.-H. Duvigneaud, T. Segato, Morphotropic phase boundary in the BNT–BT–BKT system, Ceram. Int. 38 (2012) 2823–2827.

[18] P. Jaita, A. Watcharapasorn, D.P. Cann, S. Jiansirisomboon, Dielectric, ferroelectric and electric field-induced strain behavior of $Ba(Ti_{0.90}Sn_{0.10})O_3$-modified $Bi_{0.5}(Na_{0.80}K_{0.20})_{0.5}TiO_3$ lead-free piezoelectrics, J. Alloys Compd. 596 (2014) 98–106.

[19] V.D.N. Tran, T.-H. Dinh, H.-S. Han, W. Jo, J.-S. Lee, Lead-free $Bi_{1/2}(Na_{0.82}K_{0.18})_{1/2}TiO_3$ relaxor ferroelectrics with temperature insensitive electrostrictive coefficient, Ceram. Int. 39 (2013) S119–S124.